Journal of Network Intelligence
Taiwan Ubiquitous Information
 ISSN 2414-8105 (Online)
Volume **9**, Number **3**, August **2024**

Gas Emission Prediction Based on Secondary Decomposition and MSCSO-WLSSVM

Xue-Han Zhao

School of Computer Science and Technology
Henan Polytechnic University
Jiaozuo 454000, P. R. China
376842083@qq.com

Wei-Peng An*

School of Software
Henan Polytechnic University
Jiaozuo 454000, P. R. China
212109020065@home.hpu.edu.cn

Wei-Hao Qiao

School of Computer Science and Technology
Henan Polytechnic University
Jiaozuo 454000, P. R. China
cywaniii@163.com

Chang-Zhou Lv

School of Computer Science and Technology
Henan Polytechnic University
Jiaozuo 454000, P. R. China
2597511146@qq.com

*Corresponding author: Wei-Peng An

Received June 29, 2023, revised October 11, 2023, accepted December 27, 2023.

Abstract. *This paper proposes a combined prediction model based on secondary decomposition and MSCSO-WLSSVM to enhance methane gas emission prediction accuracy. Firstly, the complete ensemble empirical mode decomposition with adaptive noise (CEEMDAN) is applied to decompose the residual term of variational mode decomposition (VMD). This effectively extracts the important information from the original data. Secondly, the global search ability and local exploitation ability of the sand cat swarm optimization algorithm (SCSO) are enhanced by introducing chaotic sequence and Lévy flight strategy. Then, the modified SCSO (MSCSO) is used to optimize kernel width and regularization parameters of the weighted least squares support vector machines (WLSSVM). Finally, the combined model MSCSO-WLSSVM is used to individually predict each decomposed subsequence, and the predicted results are then superimposed, further enhancing the overall prediction accuracy. The experimental results show this model(VCMW) has significant improvements over the SCSO-WLSSVM model, with reductions of* 84.45% *in mean square error and* 92.31% *in average relative variance. Additionally, the coefficient of determination has increased by* 26.42%*, demonstrating superior performance compared to competing models and highlighting its capability for precise and efficient gas emission prediction.*

Keywords: Methane gas emission prediction, Secondary decomposition, Sand cat swarm optimization algorithm, Weighted least squares support vector machines.

1. **Introduction.** Given the abundant coal resources within China's national territory, the reliance on coal as the primary energy source is unlikely to change in the short term [1]. However, as mining depth and intensity increase, the number of uncontrollable factors beneath the mines also rises, leading to frequent and severe coal mine accidents [2, 3]. Gas emissions, in particular, are the leading cause of such accidents [4]. These incidents compromise mine ventilation safety, posing a significant threat to the lives of construction workers. Moreover, they cause extensive damage to infrastructure and greatly reduce mining efficiency. Consequently, achieving high-precision prediction of gas emissions within mines becomes crucial. Accurate prediction allows for effective control of gas emissions, ensuring ventilation and construction safety, as well as improved mining efficiency. This pursuit holds practical significance in preventing mine accidents through proactive regulation [5, 6]. Methane gas emission time series are commonly influenced by a multitude of complex factors, including the coal seam gas content, ground atmospheric pressure, and coal seam burial depth. These factors contribute to the strong non-linear and non-smooth nature of the methane gas emission time series, which in turn poses challenges for accurate prediction.

1.1. **Related work.** The following content provides a concise literature review of the method proposed in this paper.

With the progress of time and technological advancements, artificial intelligence, digital twins, cloud computing, and other emerging technologies have emerged in recent years [7, 8, 9]. In such an environment, prediction methods based on machine learning and deep learning have been widely employed across various research domains, including the prediction of gas emissions [10, 11, 12]. Currently, gas emission prediction methods can be categorized into three main categories: traditional prediction methods, artificial intelligence prediction methods, and combined model prediction methods. Traditional prediction methods [13], such as the mine statistics method and the split-source prediction method, have gradually become less effective in the increasingly complex mining environment.

Therefore, it is imperative to explore more scientific and high-precision methods for gas emission prediction. Compared to traditional prediction methods, artificial intelligence (AI) prediction methods demonstrate higher accuracy in predicting gas emissions, particularly for nonlinear time series. The method mainly utilizes algorithms to learn the relationship between relevant influencing factors and gas emission data and then realizes the prediction based on the collected monitoring data. Researchers such as Wu et al. [14], Dong et al. [15], Chen et al. [16], and Jia et al. [17] have utilized various methods, including random forest, support vector machine (SVM), BP neural network, and multiple regression analysis, to predict gas emissions. Their studies have shown significant improvements in prediction performance, generalization ability, and prediction efficiency. However, a single model cannot adequately and effectively learn the complex nonlinear relationships between gas emission data in increasingly complex environments. Moreover, the difficulty of tuning the parameters of the multiparametric model is required to be addressed.

To address this problem, the prediction method of the combinatorial model utilizes the idea of decomposition before integration [18]. It decomposes the original sequence into several subseries, predicts each subseries separately, and finally integrates the results to obtain the final prediction result. Zeng et al. [19] decomposed the dissolved gas concentration using empirical mode decomposition (EMD) and obtained the MGWO-LSSVM

model with higher prediction performance. Nevertheless, the decomposing method utilized by Zeng et al. had the problem of modal aliasing and endpoint effect. Zhang et al. [20] used VMD to decompose the complex non-stationary methane gas concentration series. In this method, the prediction accuracy had a significant enhancement and the weakness of EMD decomposition was improved. These experimental results show a significant improvement in prediction performance compared to using only the AI prediction method. The residual term of the single decomposition of VMD still contains complex and important information that is not sufficiently decomposed, according to Tang et al. [21]. Many scholars [22, 23] have gradually tried to use secondary decomposition for numerous applications. In the study of methane gas emission prediction, Lin [24] combined seasonal and trend decomposition using loess (STL) with EEMD for the secondary decomposition of gas emission and used genetic algorithm (GA) for support vector regression (SVR) parameter optimization, greatly improving the prediction accuracy. Therefore, the combined model prediction has better generalization ability and better prediction performance than the single AI prediction method. However, in their proposed approach, the inputs to the model are predictors that are strongly correlated with the original gas emission data and do not take into account that this is not the case for the degree of correlation with decomposing subseries.

1.2. **Main contribution.** In previous research, various prediction methods for methane gas emission prediction have been proposed. However, challenges including inadequate decomposition of VMD, input indicator redundancy, and model parameters hard to tune still require resolution. Therefore, we present a combined prediction approach for gas emission prediction based on secondary decomposition and the MSCSO-WLSSVM model. The main contributions of our work are as follows:

- We utilize VMD to decompose the original gas emission data, and then use CEEMDAN to decompose the residual terms of VMD for a second time, which fully decomposes the complex time series into subseries that are easy to model and predict.
- Feature selection is applied to identify crucial predictive indicators for each component, enabling the creation of dedicated training and testing sets for each component. This is beneficial for improving prediction efficiency.
- We enhance the SCSO algorithm by incorporating chaotic sequences and Lévy flights, which enhance the global exploration and local exploitation capabilities. This enhances the algorithm's optimality-seeking performance.
- The WLSSVM parameters are optimized using the MSCSO algorithm, effectively addressing the challenge of intricate parameter tuning. This greatly enhances the predictive accuracy and efficiency of WLSSVM.
- Performance analysis and comparative experimental results indicate that the model presented in this paper possesses a high level of prediction accuracy and efficiency.

2. Secondary Decomposition Principle.

2.1. **Variational mode decomposition.** Variational mode decomposition (VMD) is a method proposed by Dragomiretskiy and Zosso [25, 26] in 2014 for the decomposition of complex non-smooth signals, which decomposes the original sequence into predefined K bandwidth-limited intrinsic mode functions (IMF) with different central frequencies by a completely non-recursive variational pattern. The algorithm principle is as follows.

Step1.

The analytic signal of each mode is derived by the Hilbert transform to obtain the one-sided spectrum. The spectrum of each mode is then convolved with the exponent

of the estimated center frequency tuning so that the spectrum of each mode is tuned to the fundamental frequency band. Then the gradient squared parametrization of the signal is used as the estimated bandwidth [26]. Constraining the value of the sum of the estimated bandwidth of each mode and the approximate equivalence of the sum of the decomposed modes to the original signal yields, the constrained variational formula is shown in Equation (1).

$$\begin{aligned} &\min_{\{\mu_k\},\{\rho_k\}} \left\{ \sum_k^K \left\| \partial_t [(\delta(t) + \frac{j}{\pi t}) * u_k(t)] e^{-j\omega_k t} \right\|_2^2 \right\} \\ &s.t. \sum_k^K u_k = f \end{aligned} \tag{1}$$

where $\{u_k\}$ and $\{\omega_k\}$ are the sets of the decomposed K modes and the corresponding central frequencies separately. $\delta(t)$ represents the unit impulse functions. f instead of the original signals.

Step2.

To find the optimal solution to Equation (1), the constrained variational problem is transformed into an unconstrained problem by introducing a quadratic penalty factor and a Lagrange multiplier operator.

$$\begin{aligned} \mathcal{L}(\{u_k\},\{\omega_k\},\lambda) := \alpha \sum_k \left\| \partial_t [(\delta(t) + \frac{j}{\pi t}) * u_k(t)] e^{-j\omega_k t} \right\|_2^2 + \left\| f(t) - \sum_k u_k(t) \right\|_2^2 \\ + \left\langle \lambda(t), f(t) - \sum_k u_k(t) \right\rangle. \end{aligned} \tag{2}$$

Step3.

Calculating the saddle point of Equation (2) when using the alternating direction multiplier method (ADMM) to iteratively update parameters, so that derive the center frequency and bandwidth at this point which is exactly the optimal solution of the original problem. The parameters are updated with the following formula.

$$\begin{aligned} \hat{u}_k^{n+1}(\omega) &= \frac{\hat{f}(\omega) - \sum_{i \neq k} \hat{u}_i(\omega) + \frac{\hat{\lambda}(\omega)}{2}}{1 + 2\alpha(\omega - \omega_k)^2}; \\ \omega_k^{n+1} &= \frac{\int_0^\infty \omega \left| \hat{u}_k(\omega) \right|^2 d\omega}{\int_0^\infty \left| \hat{u}_k(\omega) \right|^2 d\omega}; \\ \hat{\lambda}^{n+1}(\omega) &\leftarrow \hat{\lambda}^n(\omega) + \tau \left(\hat{f}(\omega) - \sum_k \hat{u}_k^{n+1}(\omega) \right). \end{aligned} \tag{3}$$

After setting the value of K and initializing the parameters in Equation (3), start updating u_k and ω_k, which in turn obtains the value of λ. Stop the iteration if the following condition is met, otherwise, continue updating and ω_k.

$$\sum_k \frac{\|\hat{u}_k^{n+1} - \hat{u}_k^n\|_2^2}{\|\hat{u}_k^n\|_2^2} < \epsilon \tag{4}$$

where $\hat{u}_k^n$, $\hat{f}_k(\omega)$, and $\hat{\lambda}^n$ are the results of the Fourier transform of u_k^n, $f(t)$ and λ^n respectively. ϵ is larger than 0 and represents the determination accuracy.

Step4.

After obtaining each IMF after decomposition, the residual term of the decomposition can be found according to Equation (5).

$$res = f(t) - \sum_{i=1}^{k} u_i(t) \tag{5}$$

2.2. **Complete ensemble empirical mode decomposition with adaptive noise.** CEEMDAN is an improved method based on empirical modal decomposition (EMD) proposed by María E. Torres et al in 2011 [27, 28]. The problem of modal mixing that occurs in EMD is effectively improved and the reconfigurability of the signal is enhanced to a greater extent by introducing adaptive Gaussian white noise and using multiple superpositions to find the mean value.

Let $R(t)$ be the residual sequence after primary decomposition that is the original sequence of secondary decomposition, $E_i(\cdot)$ be the i-th order modal function obtained by EMD decomposition, ε be the adaptive factor for each addition of Gaussian white noise, $\omega_i(t)$ be the Gaussian white noise added to the original sequence for the i-th time and CMF_j be the j-th order modal component obtained by CEEMDAN decomposition. Then, the principle and steps of the secondary decomposition using CEEMDAN are as follows.

Step1.

In the first iteration, N times of adaptive Gaussian white noise are added to $R(t)$ to obtain the following signal to be decomposed.

$$R_i(t) = R(t) + \varepsilon_0 \omega_i(t),\ i \in [1, N] \tag{6}$$

Step2.

The EMD decomposition is performed separately for the signal to be decomposed in the above equation and the corresponding i-th order modal components are taken, and then the sum of these N modal components is averaged to obtain CMF_1. The residual term of the first iteration $r_1(t)$ is then obtained.

$$\begin{gathered} CMF_1 = \frac{\sum_{i=1}^{N} E_i\left(R_i(t)\right)}{N} = \frac{\sum_{i=1}^{N} E_i\left(R(t) + \varepsilon_0 \omega_i(t)\right)}{N}; \\ r_1(t) = R(t) - CMF_1. \end{gathered} \tag{7}$$

Step3.

In the second iteration, the signal to be decomposed is obtained by adding N times of adaptive Gaussian white noise to $r_1(t)$.

$$r_1^i(t) = r_1(t) + \varepsilon_1 E_1\left(\omega_i(t)\right) \tag{8}$$

Step4.

Carry out step 2 for these N signals to be decomposed, and then obtain CMF_2 and $r_2(t)$ with the following equations.

$$\begin{gathered} CMF_2 = \frac{\sum_{i=1}^{N} E_i\left(r_1^i(t)\right)}{N} = \frac{\sum_{i=1}^{N} E_i\left(r_1(t) + \varepsilon_1 E_1(\omega_i(t))\right)}{N}; \\ r_2(t) = r_1(t) - CMF_2. \end{gathered} \tag{9}$$

Step5.

Repeating the operations of steps 3 and 4 for the remaining K-2 iterations yields CMF_{j+1} and $r_{j+1}(t)$ with the following equations.

$$\begin{aligned} CMF_{j+1} &= \frac{\sum_{i=1}^{N} E_i\left(r_j^i(t)\right)}{N} = \frac{\sum_{i=1}^{N} E_i\left(r_j(t) + \varepsilon_j E_j(\omega_i(t))\right)}{N}; \\ r_{j+1}(t) &= r_j(t) - CMF_{j+1}, j \in [1, K-1]. \end{aligned} \tag{10}$$

Step6.

The iteration is terminated until the restriction of the residual term (the number of poles is not more than 2) is satisfied by repeating K iterations, and finally, the residual term r_K of the CEEMDAN decomposition is obtained.

$$r_K(t) = R(t) - \sum_{k=1}^{K} CMF_k \tag{11}$$

Then, the residual term $R(t)$ after the primary decomposition is decomposed by CEEMDAN, which can be expressed as follows.

$$R(t) = \sum_{k=1}^{K} CMF_k + r_K(t) \tag{12}$$

The principle of CEEMDAN decomposition can be represented by FIGURE 1 as follows.

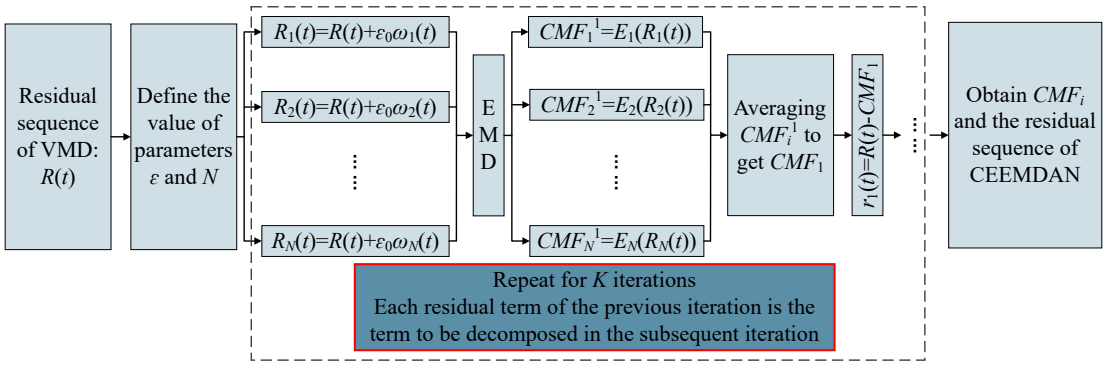

FIGURE 1. Schematic diagram of the CEEMDAN principle.

3. Principle of Prediction Model Based on MSCSO-WLSSVM.

3.1. **Sand cat swarm optimization algorithm.** SCSO algorithm is inspired by sand cats with a highly sensitive hunting mechanism for low-frequency signals [29]. Unlike domestic cats, the sensitivity of sand cats is 8 dB higher than that of domestic cats in environments below 2 kHz [30]. Living in a harsh desert environment for a long time, the hunting mechanism of sand cats is mainly divided into two phases: search and attack. Because it often hunts for individuals, the SCSO algorithm assumes that the sand cat hunts in groups, thus reinforcing the concept of group intelligence optimization.

3.1.1. *Standard SCSO algorithm.* The specific steps of the standard SCSO algorithm are derived from the literature [29] and are divided into four main phases: the initial population phase, searching the prey (exploration) phase, attacking the prey (exploitation) phase, and the balance between the exploration and exploitation phase. The specific implementation principles and steps of the SCSO algorithm are as follows.

Step1. Initial population.

Firstly, the candidate matrix that is the candidate solutions to the problem is determined with each sand cat as a candidate. As shown in FIGURE 2, it represents the working mechanism of the SCSO algorithm in each iteration of the initialization phase. The dimensions of this matrix are determined by the number of sand cats within the population and the dimensions of the problem to be solved, and each variable $(x_1, x_2, ..., x_d)$ is a floating-point number whose value is randomly generated between the upper and lower bounds x , $\forall x_i \in [x_{min}, x_{max}]$.

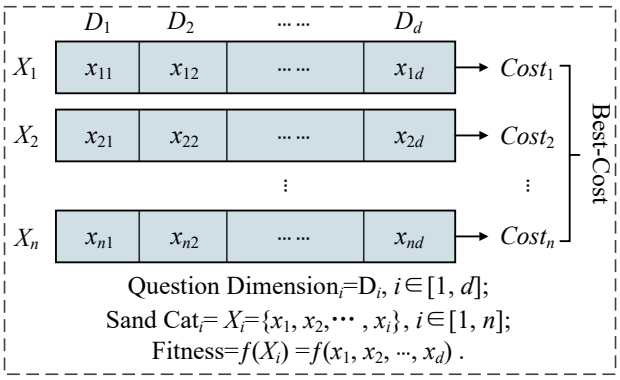

FIGURE 2. The working mechanism of the SCSO algorithm.

Secondly, the fitness value of each sand cat is calculated to obtain the best solution. The fitness value for each sand cat is calculated by using a specific fitness function separately. The sand cat with the smallest fitness value at the end of each iteration is taken as the optimal solution in the current state, and the other sand cats in the population approach this candidate in subsequent iterations to find the optimal solution to the problem.

Step2. Searching the prey (exploration).

Since the SCSO algorithm is mainly inspired by the high sensitivity of the sand cat to low-frequency signals, especially the advantage is more obvious within the environment below 2 kHz, the SCSO algorithm sets the sensitivity range of the sand cat within 2 kHz and expresses each candidate solution as $X_i = (x_{i1}, x_{i2}, ..., x_{id}), i \in [1, n]$. If the sensitivity range of the sand cat population is represented by the parameter $\overrightarrow{r_G}$ and this parameter decreases linearly from 2 to 0 in each iteration, the equation is expressed as:

$$\overrightarrow{r_G} = s_M - \frac{s_M \times iter_c}{iter_{Max}} \tag{13}$$

where s_M is a parameter defined by the auditory characteristics of the sand cat, so the value is 2; $iter_c$ denotes the current number of iterations; $iter_{Max}$ denotes the maximum number of iterations.

To avoid local optimum, the sensitivity range of each sand cat in the search and attack phases is denoted by $\overrightarrow{r}$ and calculated with the following formula.

$$\overrightarrow{r} = \overrightarrow{r_G} \times rand(0, 1) \tag{14}$$

In the process of searching for prey, each sand cat updates its position based on the current best candidate position $\overrightarrow{Pos_{bc}}$, its current position $\overrightarrow{Pos_c}$, and its sensitivity range $\overrightarrow{r}$, which this search mechanism can be expressed by Equation (15).

$$\overrightarrow{Pos}(t+1) = \overrightarrow{r} \cdot \left(\overrightarrow{Pos_{bc}}(t) - rand(0, 1) \cdot \overrightarrow{Pos_c}(t)\right) \tag{15}$$

Step3. Attacking on the prey (exploitation).

The SCSO algorithm uses a roulette strategy to generate a random angle ($0° \leq \theta \leq 360°$) between the next random position $\overrightarrow{Pos_{rnd}}$ of each sand cat and the current position so that $cos(\theta)$ in formula 16 is between -1 and 1. Also, such randomness allows the sand cat to avoid falling into the trap of local optimality, and this mechanism of approaching the prey (seeking the optimal solution) is expressed as follows.

$$\begin{aligned} \overrightarrow{Pos_{rnd}} &= \left| rand(0,1) \cdot \overrightarrow{Pos_b}(t) - \overrightarrow{Pos_c}(t) \right|, \\ \overrightarrow{Pos}(t+1) &= \overrightarrow{Pos_b}(t) - \overrightarrow{r} \cdot \overrightarrow{Pos_{rnd}} \cdot \cos(\theta). \end{aligned} \tag{16}$$

Step4. The balance between exploration and exploitation.

To make the transition between the prey search phase and the attack phase of the sand cat more balanced, an adaptive factor $\overrightarrow{R}$ was introduced and denoted as follows.

$$\overrightarrow{R} = 2 \times \overrightarrow{r_G} \times rand(0,1) - \overrightarrow{r_G} \tag{17}$$

By adaptive switching of $\overrightarrow{r_G}$ and $\overrightarrow{R}$, the sand cat position update strategy in the balance phase of search and attack is as follows.

$$\overrightarrow{X}(t+1) = \begin{cases} \overrightarrow{Pos_b}(t) - \overrightarrow{Pos_{md}} \cdot \cos(\theta) \cdot \overrightarrow{r} & |\overrightarrow{R}| \leq 1 \\ \overrightarrow{r} \cdot \left(\overrightarrow{Pos_{bc}}(t) - rand(0,1) \cdot \overrightarrow{Pos_c}(t) \right) & |\overrightarrow{R}| > 1 \end{cases} \tag{18}$$

where the sand cat is close to the target when $|\ \overrightarrow{R}\ | \leq 1$, so it enters the attack phase and updates its position with the strategy of Equation (16); the sand cat is still far from the target when $|\ \overrightarrow{R}\ | > 1$, so it enters the target search phase and updates its position with the strategy of Equation (15).

3.1.2. *Modified SCSO algorithm.* The SCSO algorithm is easy to implement with few parameters and the sensitivity of individuals is strong, but it has the following defects: the initial position of the randomly generated population lacks diversity leading to the limited global exploration ability; it is easy to fall into the trap of local optimum, thus the search stagnation phenomenon occurs, so the local exploitation ability needs to be improved. The SCSO algorithm is improved by the following two aspects.

Step1. Embedding Tent Chaos Sequence.

Chaotic sequences are nonlinear phenomena prevalent in nature, which are characterized by pseudo-randomness, ergodicity, and unpredictability [31]. This property of chaotic sequences is exploited to map the randomly generated initial positions in the algorithm into the chaotic space to make the initialized population positions more uniform, thus increasing the population diversity and enhancing the global exploration ability of the algorithm [32]. The common chaotic mappings are Logistic mapping, Tent mapping, and so on [33]. There are extensive studies showing that Logistic mappings are less effective than Tent mappings in traversal uniformity, which can lead to slower convergence [34]. In this paper, we use Tent mapping for population location initialization, and Tent mapping denotes as follows.

$$x_{i+1} = \begin{cases} 2x_i & 0 \leq x_i \leq 0.5 \\ 2(1-x_i) & 0.5 < x_i \leq 1 \end{cases} \tag{19}$$

where the Tent mapping parameter α is configured as 0.5 to obtain a more uniformly distributed sequence, which makes the initial position of the population more uniform, expands the search range of the sand cat in space, increases sand cat population diversity, enhances the global exploration ability of the SCSO algorithm in the early stage, and to

a certain degree avoids the problems of this algorithm being premature and easy to fall into local optimum.

Step2. Local search strategy based on Lévy flight.

Lévy flight is a random wandering search strategy, which is more efficient than the Brownian random wandering search strategy [35]. The method utilizes its unique combined motion characteristics of a large number of short-step searches and a small number of long-step jumps to be able to expand the search range, perturb at local stuck optima and search stagnation to enable it to jump out of local optima [36], and finally make the SCSO algorithm achieve a better balance between the searching phase (exploration) and the attacking phase (exploitation) to obtain faster and better algorithmic search results. Therefore, one Lévy flight is performed after each sand cat position update, and the position update is performed according to Equation (20).

$$x_{id}(t+1) = x_{id}(t) + \alpha \oplus Levy(\lambda) \tag{20}$$

where $x_{id}(t)$ denotes the position of sand cat i in the d-th dimension of the t-th iteration, α denotes the control step weight coefficient and $Levy(\lambda)$ denotes the random wandering path that conforms to the Lévy flight. Where the Lévy flight conforms to the following distribution.

$$Levy(\lambda) \sim u = t^{-\lambda}, \quad (1 < \lambda < 3) \tag{21}$$

Mantegna proposes to calculate the random steps of the Lévy flight. The calculation formula is shown in Equation (22).

$$Levy(\lambda) = \frac{\varphi \times u}{\mid \nu \mid^{1/\lambda}} \tag{22}$$

where $Levy(\lambda)$ denotes the random step of Lévy flight; λ is usually taken as 1.5; u and v conform to the normal distribution of Equation (23) respectively, and φ is the variance.

$$\begin{cases} u \sim N(0, \varphi_u^2) \\ \nu \sim N(0, \varphi_\nu^2) \end{cases} \tag{23}$$

If the gamma function is denoted by Γ, the variances of φ_u and φ_v are defined as Equation (24).

$$\begin{cases} \varphi_u = \left\{ \dfrac{\Gamma(1+\lambda) \cdot \sin(\pi \cdot \lambda/2)}{\Gamma[(1+\lambda)/2] \cdot \lambda \cdot 2^{(\lambda-1)/2}} \right\}^{1/\lambda} \\ \varphi_\nu = 1 \end{cases} \tag{24}$$

3.2. **Weighted least squares support vector machine.** LSSVM reduces the complexity of the problem to a greater extent by introducing two-norms into the objective function and using equation constraints instead of the traditional support vector machine (SVM) inequality constraint-solving method [37, 38]. However, since all Lagrange multipliers in the LSSVM solution process are nonzero and the entire training set is involved in each prediction, the LSSVM model lacks sparsity and robustness performance. To address this deficiency, WLLVM matches the error of LSSVM with the corresponding weight as a way to mitigate the adverse effects of noise and speed up the convergence of the model [39, 40]. The specific implementation principles and steps of WLSSVM are as follows.

Step1.

Given a training set $\{x_i, y_i\},\ i \in [1, N]$, where x_i is the d-dimensional input data and y_i is the one-dimensional output data. The error variable e_i is obtained during the solution of the LSSVM, and the specific steps are described in the literature [37]. The weight

coefficient v_i assigned to e_i is calculated from the sample training error and is given by the following formula.

$$\nu_i = \begin{cases} 1 & \text{if } \mid e_i/\hat{s} \mid \leq c_1, \\ \frac{c_2 - |e_i/\hat{s}|}{c_2 - c_1} & \text{if } c_1 \leq \mid e_i/\hat{s} \mid \leq c_2, \\ 10^{-4} & \text{otherwise.} \end{cases} \tag{25}$$

where c_1 and c_2 are usually taken as 2.5 and 3; $\hat{s}$ is represented by the following equation; IQR is the difference between the third quartile and the first quartile after sorting the error e_i from smallest to largest.

$$\hat{s} = IQR/(2 * 0.6745) \tag{26}$$

Step2.

After knowing the error variables e_i and the corresponding weights v_i, the following WLSSVM model is obtained.

$$\begin{cases} \min\limits_{\omega,e,b} J(\omega, e) = \dfrac{1}{2}\omega^T\omega + \dfrac{1}{2}\lambda \sum\limits_{i=1}^{N} \nu_i e_i^2 \\ s.t.\ y_i = \omega^T\phi(x_i) + b + e_i,\ i \in [1, N] \end{cases} \tag{27}$$

where ω is the weight vector in the original weight space, λ is the regularization parameter, $\phi(\cdot)$ is the function that maps the input space to the high-dimensional feature space, and b is the bias.

Step3.

Equation (27) can be transformed into the following equation by introducing the Lagrangian function.

$$L(\omega, b, e, \alpha^*) = \frac{1}{2}\omega^T\omega + \frac{1}{2}\lambda \sum_{i=1}^{N} \nu_i e_i^2 - \sum_{i=1}^{N} \alpha_i^* [\omega^T\phi(x_i) + b + e_i - y_i] \tag{28}$$

where α_i^* is a sequence of Lagrange multipliers.

Step4.

To solve Equation (28), the radial basis function (RBF) is introduced according to the KKT (Karush-Kuhn-Tucker) optimality condition.

$$K(x_i, x_j) = \exp(-\frac{\parallel x_i - x_j \parallel^2}{2\sigma}) \tag{29}$$

This simplifies the inner product operation in the feature space and transforms the optimization problem into the following form.

$$\begin{pmatrix} 0 & l_{1\times N} \\ l_{N\times 1} & K + V_\lambda \end{pmatrix} \begin{pmatrix} b \\ \alpha^* \end{pmatrix} = \begin{pmatrix} 0 \\ y \end{pmatrix} \tag{30}$$

where $l_{1\times N}$ is a $1 \times N$ unit row vector; $l_{N\times 1}$ is an $N \times 1$ unit column vector; α^* is a sequence of Lagrange multipliers, and y is the output data, both of which are $1 \times N$ column vectors;

$$\begin{aligned} K &= K(x_i, x_j) = \phi(x_i)^T \cdot \phi(x_j); \\ V_\lambda &= diag\{\frac{1}{\lambda\nu_1}, \frac{1}{\lambda\nu_2}, \cdots, \frac{1}{\lambda\nu_N}\}. \end{aligned} \tag{31}$$

where $i, j = 1, 2, ..., N$.

Step5.

Ultimately, the WLSSVM model can be represented as follows.

$$y = \sum_{i=1}^{N} \alpha_i^* K(x, x_i) + b \tag{32}$$

3.3. **MSCSO-WLSSVM prediction model construction.** To enhance the prediction accuracy of the WLSSVM model, this paper proposes optimizing the parameters of the WLSSVM prediction model using the modified sand cat swarm optimization (MSCSO) algorithm. The goal is to determine the most suitable model parameters for the raw data of methane gas emissions. The parameters to be optimized include the penalty parameters C_1 and C_2, gaussian kernel width σ, and regularization parameters λ, especially the combined values of σ and λ are very critical to the prediction accuracy and generalization ability of the model. The specific construction process of this model is as follows.

Step1.

Data preprocessing. The methane gas emission data is normalized and the dataset is divided. Subsequently, the correlation between each component and various prediction indicators is calculated, and the influential prediction indicators are selected as the feature set for that component.

Step2.

Initialize the parameters of the MSCSO algorithm, including the number of sand cat populations, the maximum number of iterations, the sensitivity range of sand cat populations and individuals, and the adaptive factor.

Step3.

During the population initialization stage, the population is mapped to the chaotic space using the Tent chaotic sequence, resulting in a more evenly distributed initial position, and the fitness value of each individual is calculated.

Step4.

During the iteration process, the updating strategy for the sand cat positions is determined based on the magnitude of the fitness factor, and after each position update, a Lévy flight is introduced to escape local optima.

Step5.

The individual with the minimum fitness value in each iteration is selected as the current best solution and compared with the best solution from the previous iteration to obtain a superior solution. This process continues until the iteration is complete, resulting in the identification of the optimal solution.

Step6.

The optimal fitness value of the MSCSO algorithm is used as the optimal input for the key parameters of the WLSSVM model, leading to the construction of the MSCSO-WLSSVM methane gas emission prediction model with superior performance. The construction process is illustrated in FIGURE 3.

4. Experimental Procedure and Results Analysis.

4.1. **Data standardization and evaluation indexes.** A total of 662 sets of methane gas emission monitoring data were collected from January 25, 2022, to February 25, 2022, at a working face in a coal mine located in Jincheng, Shanxi. The experiment involved a comprehensive analysis of the influencing factors and the actual conditions related to methane gas emission. The prediction target was the methane gas emission denoted as $Y(m^3 \cdot min^{-1})$, and the following nine influencing factors were selected as prediction indices: coal seam burial depth $X_1(m)$, coal seam gas content $X_2(m^3 \cdot t^{-1})$, coal seam thickness $X_3(m)$, inter-seam lithology X_4, working face extraction rate X_5, working face

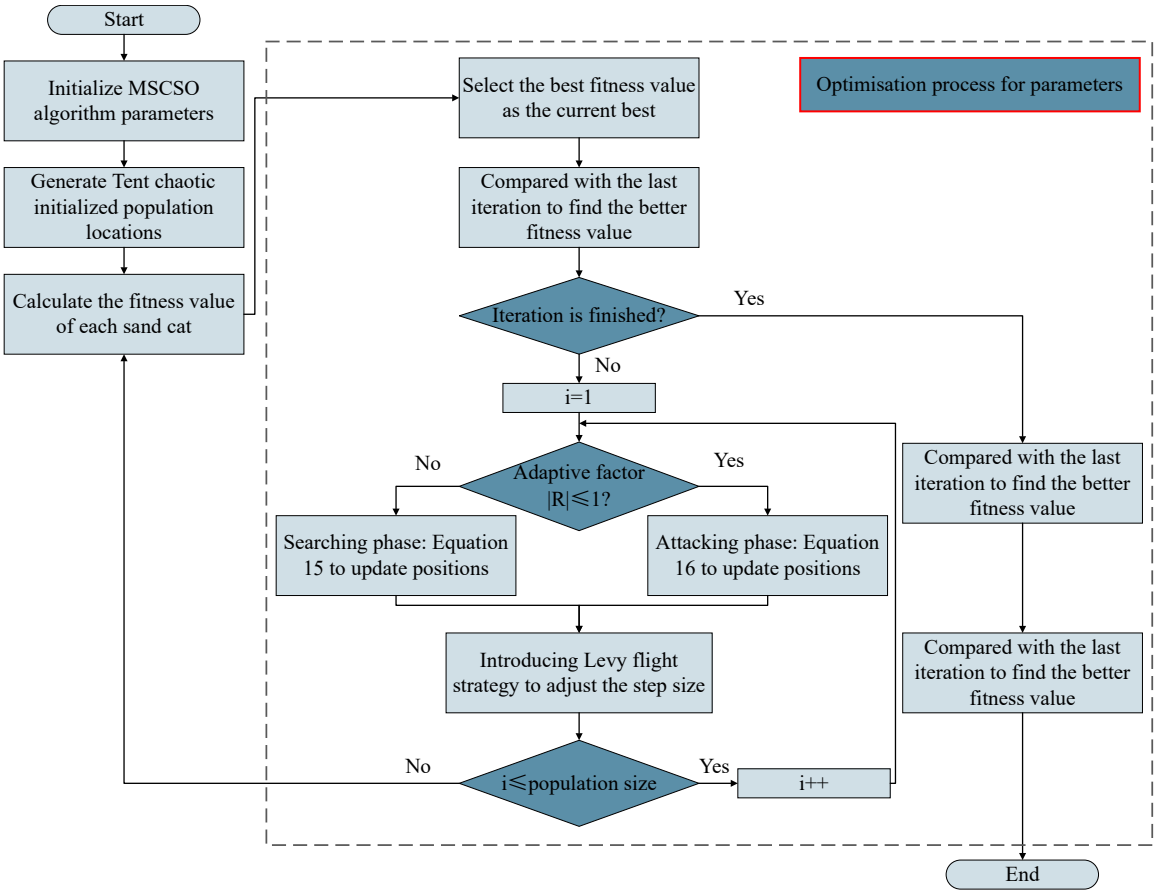

FIGURE 3. Flow chart of MSCSO-WLSSVM prediction model construction.

length $X_6(m)$, coal seam inclination $X_7(^\circ)$, neighboring seam gas content $X_8(m^3 \cdot t^{-1})$, and thickness of the adjacent seam $X_9(m)$. The first 600 data points were utilized as the training set, while the remaining 62 data points were designated as the test set. A portion of the data is presented in Table 1 below.

TABLE 1. Partial raw data on methane gas emission and predictive metrics

Serial number	X_1	X_2	X_3	X_4	X_5	X_6	X_7	X_8	X_9	Y
1	383	2.19	2.2	4.54	0.95	152	10	2.07	1.25	3.26
2	397	2.06	2.1	4.32	0.95	149	11	1.85	1.20	2.97
3	408	2.24	2.4	4.25	0.95	165	11	2.29	1.46	3.55
4	410	2.31	2.3	4.38	0.95	157	11	2.33	1.58	3.68
5	430	2.53	2.6	4.41	0.95	172	12	2.42	1.72	4.23
6	473	2.87	2.7	4.52	0.94	168	13	2.58	1.87	4.76
7	497	2.82	2.7	4.66	0.95	171	15	2.37	1.87	4.58
8	536	3.53	3.0	4.73	0.94	176	12	2.93	1.69	5.34
9	568	3.91	3.4	4.61	0.92	180	13	3.16	1.74	5.73
10	572	3.76	3.4	4.53	0.93	169	13	2.89	1.53	5.34

Each influencing factor of the dimension of the collecting dataset is different. To avoid the error caused by different scales, the data need to be standardized before training the

WLSSVM model, and this paper uses the Min-Max normalization method.

$$X_{scale} = \frac{X - X_{min}}{X_{max} - X_{min}} \tag{33}$$

where X and X_{scale} denote the monitored raw data and the normalized data respectively; X_{max} and X_{min} represent the maximum and minimum values of the original data. Besides, the prediction results outputted need to reverse normalized according to the following formula.

$$X^{'} = X_{scale}(X_{max} - X_{min}) + X_{min} \tag{34}$$

where X' is the prediction result of gas emission after inverse normalization. In this paper, root mean square error ($RMSE$), average relative variance (ARV), and coefficient of determination (R^2) are chosen as the evaluation indexes of the gas emission prediction model.

$$e_{RMSE} = \sqrt{\frac{1}{\mathrm{N}}\sum_{i=1}^{N}(X_i - X_i')^2}, e_{ARV} = \frac{\sum_{i=1}^{N}(X_i - X_i')^2}{\sum_{i=1}^{N}(X_i - \overline{X_i})^2}, e_{R^2} = 1 - \frac{\sum_{i=1}^{N}(X_i' - X_i)^2}{\sum_{i=1}^{N}(\overline{X_i} - X_i)^2}. \tag{35}$$

where X_i is the true value of gas emission; $X_i^{'}$ is the predicted value of gas emission; $\overline{X_i}$ is the mean value of the original gas emission data; N is the test sample size. e_{RMSE} is used to evaluate the prediction accuracy of the model, if the smaller the value, the higher the prediction accuracy of the model; e_{ARV} is used to judge the generalization ability of the model, the smaller the value represents the stronger the generalization ability of the model; e_{R^2} is also known as the degree of fit, generally used to calculate the correlation between the predicted value and the true value, if the value is closer to 1, it means that the better the fit of the gas emission prediction model, and conversely, the worse the fit.

4.2. **Secondary decomposition and forecasting process.**

4.2.1. *The process and analysis of secondary decomposition.* Since the number of modal components K obtained from the VMD decomposition has a large impact on the prediction effect of the subsequent model, the most suitable K value for the data sample should be selected to avoid the undesirable effects caused by the improper value of K. If the K value is too small, it will lead to insufficient decomposition of the data and the complexity of the data cannot be effectively reduced; on the contrary, it will lead to over-decomposition of the data and thus reduce the prediction efficiency. In the best condition, the center frequencies of each modal component will not overlap, and Figure 4 shows the center modal situation of each IMF when K is set to 6. If K is greater than 6, the central frequencies will overlap (over decomposition), and the limit of decomposition has been reached when K=6, so 6 is selected as the number of modal components in VMD.

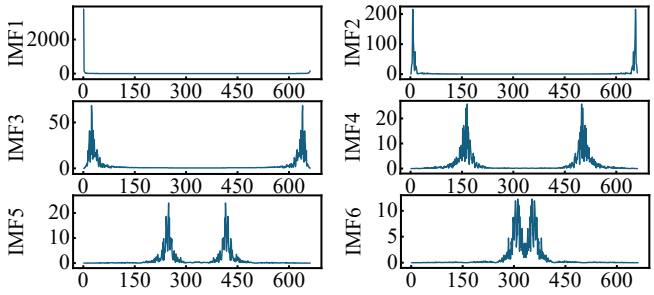

Figure 4. Spectrogram of the central mode when K is set to 6 in the VMD.

Furthermore, the parameter τ in the VMD decomposition significantly affects the prediction accuracy, and different values can result in varying degrees of prediction error [41]. By evaluating the K-component series U_k and calculating the root mean square error ($RMSE$) of the original gas emission data Y, the optimal value (REI) for the parameter τ can be determined using Equation (36).

$$\tau = \min \frac{1}{N} \sum_{i=1}^{N} \left| \sum_{k=1}^{K} U_k - Y \right|_i \tag{36}$$

Once the parameters are defined, the original gas emission data undergoes VMD decomposition. The resulting decomposed residual sequence is then subjected to a two-step decomposition using CEEMDAN. The decomposition process is illustrated in FIGURE 5.

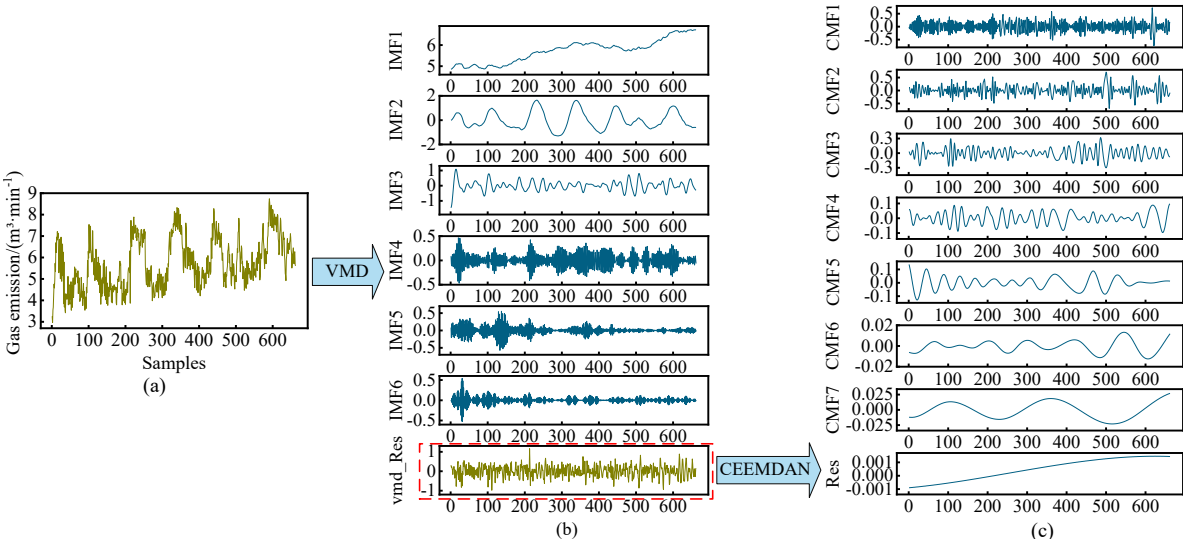

FIGURE 5. Realization process of secondary decomposition. (a)Original data on gas emission, (b)Gas emission decomposition using VMD, (c)Residual term decomposition using CEEMDAN.

4.2.2. *Forecasting process.* The methane gas emission presents a non-linear change pattern due to the complex factors under the mine. If the traditional prediction method is adopted, it will lead to high prediction error and low accuracy. In this paper, we use VMD to decompose firstly the original methane gas emission data. In addition, the decomposed residual term vmd_Res contains a large amount of important information, and by using CEEMDAN for its second decomposition, the effective decomposition of the important information of the original data is achieved. In addition, the parameters of the WLSSVM model are optimized using the MSCSO algorithm, to complete the modeling and predicting of each component after decomposition. Finally, the prediction results obtained above are added to obtain the prediction results of the original sequence. The whole process and results of the prediction are shown in FIGURE 6.

The specific prediction steps are as follows.

Step1.

Using the VMD signal decomposition technique, the first decomposition of the original data of methane gas emission is carried out to obtain the decomposition components IMFs and the residual term vmd_Res.

Step2.

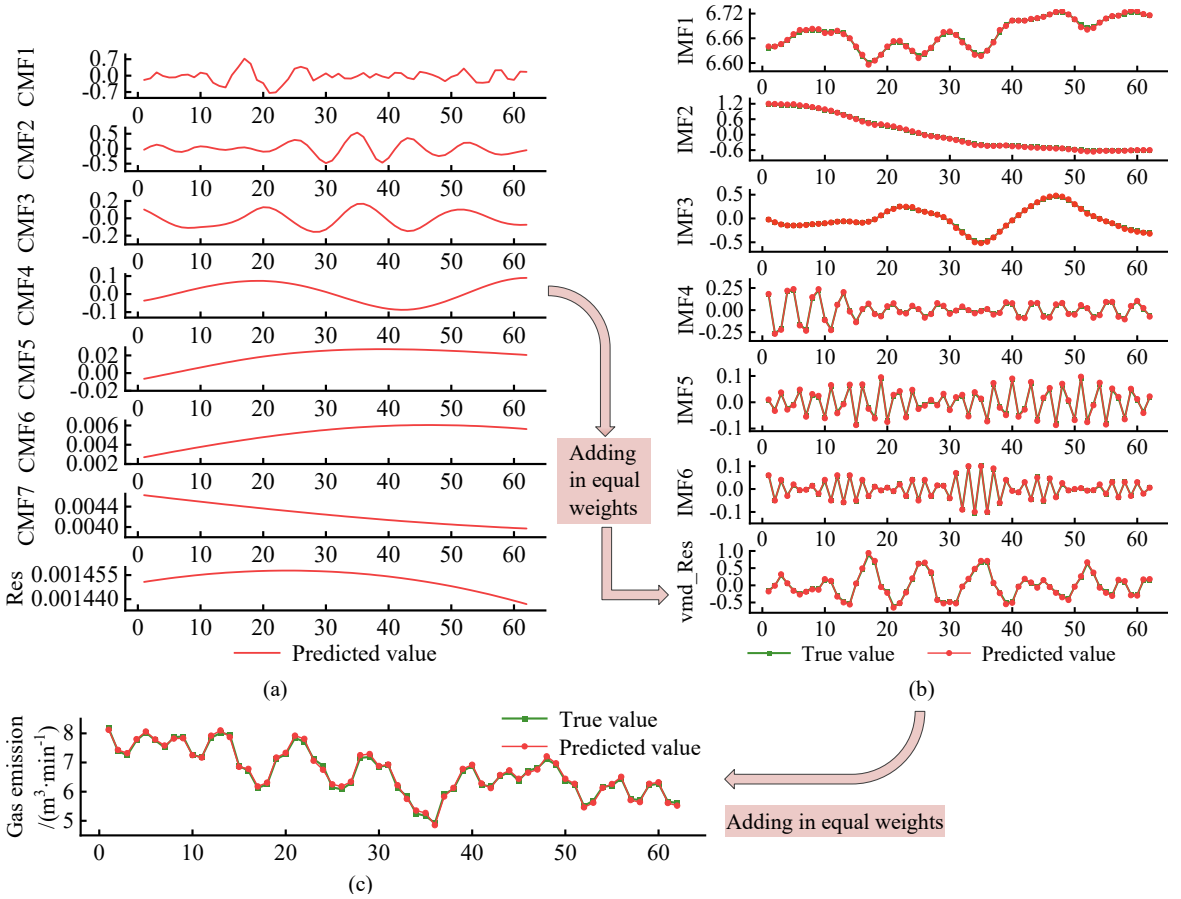

FIGURE 6. The gas emission prediction process of VMD-CEEMDAN-MSCSO-WLSSVM. (a)CEEMDAN components and residual predictions, (b)VMD components and residual predictions, (c)Predicted gas emission results for testing samples.

The correlation between each IMF and the influencing factors is computed, and the strongly correlated factors are selected as the feature set for each IMF. Subsequently, utilizing the modeling approach outlined in Section 3.3, MSCSO-WLSSVM prediction models specific to each IMF are constructed. These models are then employed to individually predict each IMF component, resulting in the corresponding prediction results obtained sequentially, as depicted in FIGURE 6 (b).

Step3.

The residual term vmd_Res obtained from the VMD decomposition is further decomposed using the CEEMDAN signal decomposition technique, resulting in the decomposition components CMFs and the residual term Res.

Step4.

Similar to Step 2, the MSCSO-WLSSVM prediction models were constructed for each CMF and Res obtained from the CEEMDAN. Subsequently, each component was individually predicted to obtain the corresponding prediction values, and the prediction results are presented in FIGURE 6 (a).

Step5.

The predicted values of each component obtained in Step 2 and Step 4 are combined using equal weights to obtain the final gas emission prediction results.

The key parameters for the VMD-CEEMDAN-MSCSO-WLSSVM gas emission prediction model proposed in this paper are set as shown in Table 2. Meanwhile, the key

parameters of the WLSSVM model Gaussian kernel width and regularization parameter are set as $\sigma^2 \in [0.01, 10]$ and $\lambda \in [0.01, 600]$ separately. The optimal combination of the above two hyperparameters can be derived as $\sigma^2 = 2.371$ and $\lambda = 197.32$ by using the MSCSO optimization algorithm to find the optimal combination of parameters. After setting the parameters, the optimal parameter combination is used to train the model again. Subsequently, the model is tested using the test samples to evaluate its performance.

TABLE 2. Key parameters of the gas emission prediction model

Key parameters	value
K	6
Bandwidth limitation	2000
Random seed	7
Kernel function	RBF
The initial number of population	80
Maximum number of iterations	100
Maximum number of chaotic iterations	200
Cycle termination times	50

The construction flowchart of the proposed methane gas emission prediction model is illustrated in FIGURE 7. The process of building the MSCSO-WLSSVM model is presented in Section 3.3.

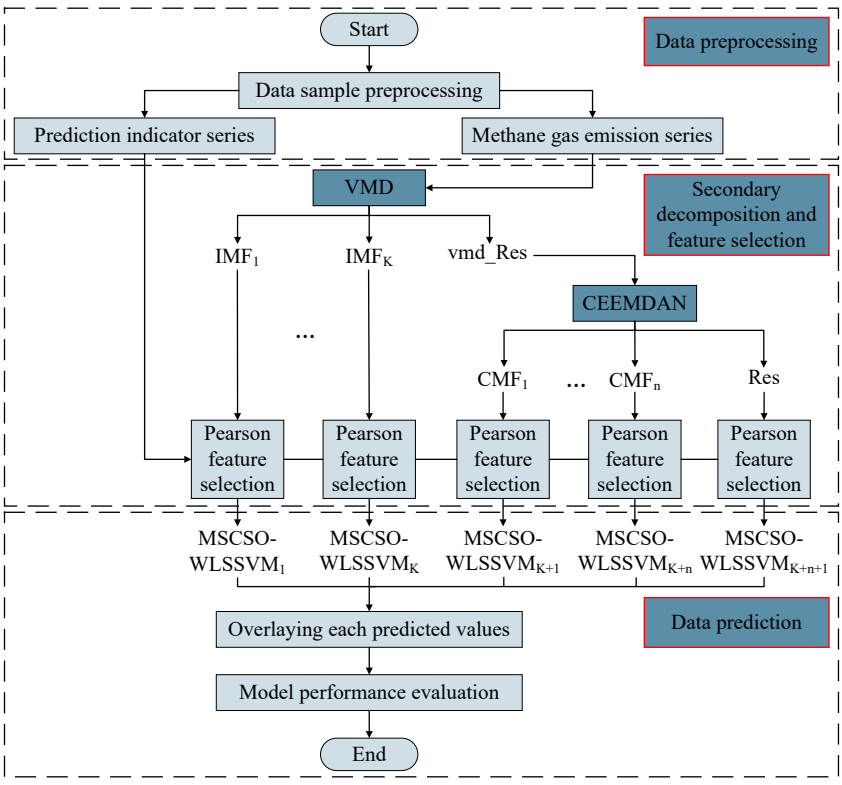

FIGURE 7. VMD-CEEMDAN-MSCSO-WLSSVM gas emission prediction flow chart.

4.3. **Algorithm performance analysis and comparison experiments.**

4.3.1. *MSCSO algorithm performance analysis.* To verify the optimization performance of the MSCSO algorithm, this study compares its performance with particle swarm optimization (PSO), genetic algorithm (GA), grey wolf optimization algorithm (GWO), and the standard sand cat swarm optimization algorithm (SCSO). The following parameter settings were used for the comparison experiments: In the PSO algorithm, the search coefficients were set as c_1=1.6 and c_2=1.7, and the inertia weight was set as ω=0.4. In the GA algorithm, the mutation probability was set as 0.01 and the crossover probability was set as 0.7. In the GWO algorithm, the search coefficient C was set as 1.4. For both the SCSO and MSCSO algorithms, the individual sensitivity range $\overrightarrow{r_G}$ was set as 2, the chaotic factor α was set as 0.4, and the parameter λ was set as 1.5. The population size for all five optimization algorithms was set as 80, and the maximum number of iterations was set as 100. The fitness value changes with the number of iterations are shown in Figure 8.

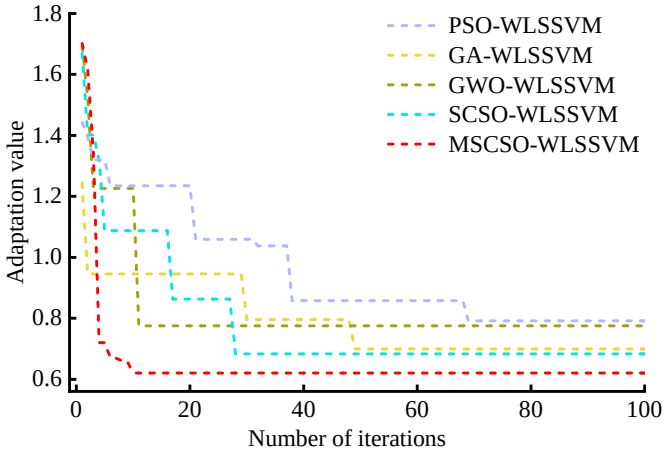

Figure 8. Fitness iteration curve of 5 optimization algorithms.

From Figure 8, it is evident that the PSO algorithm has high fitness values and tends to get trapped in local optima. It also exhibits the slowest convergence speed among the five algorithms. The GA algorithm shows some improvement in convergence speed and optimization ability compared to PSO, but its overall performance is still poor for finding the optimal WLSSVM parameter combination. The GWO algorithm has significantly improved convergence speed, but it does not yield satisfactory fitness values, indicating limited optimization performance. The SCSO algorithm achieves fitness values similar to GA after convergence but has a slight advantage in convergence speed. However, it still has room for improvement. In contrast, the MSCSO algorithm reaches convergence by the 10th iteration and demonstrates the lowest fitness values. Among the five algorithms, the MSCSO algorithm shows the best optimization performance.

In summary, the MSCSO algorithm outperforms the other algorithms in terms of convergence speed and solution quality. It effectively addresses the limitations of traditional optimization algorithms, making it a promising approach for obtaining optimal parameter combinations for the WLSSVM model.

4.3.2. *Comparison of experiments results and analysis.* To validate the effectiveness of VMD-CEEMDAN-MSCSO-WLSSVM gas emission prediction models proposed in this paper, a comparative experiment was conducted with several reference models including LSSVM, WLSSVM, SCSO-WLSSVM, MSCSO-WLSSVM, VMD-MSCSO-WLSSVM,

CEEMDAN-MSCSO-WLSSVM, and CEEMDAN-VMD-MSCSO-WLSSVM. The performance of these models was analyzed in terms of $RMSE$, ARV and R^2. The results are presented in Table 3, and the corresponding prediction results of the different models in the comparative experiments are illustrated in Figure 9.

Table 3. Comparative experimental results of different models

Serial number	Prediction models	$RMSE$	ARV	R^2
1	LSSVM	2.3801	0.0548	0.5812
2	WLSSVM	1.8046	0.0471	0.6797
3	SCSO-WLSSVM	1.3095	0.0273	0.7801
4	MSCSO-WLSSVM	0.5236	0.0142	0.8759
5	VMD-MSCSO-WLSSVM	0.4182	0.0057	0.9343
6	CEEMDAN-MSCSO-WLSSVM	0.4329	0.0062	0.8876
7	CEEMDAN-VMD-MSCSO-WLSSVM	0.3912	0.0038	0.9445
8	VMD-CEEMDAN-MSCSO-WLSSVM	**0.2036**	**0.0021**	**0.9862**

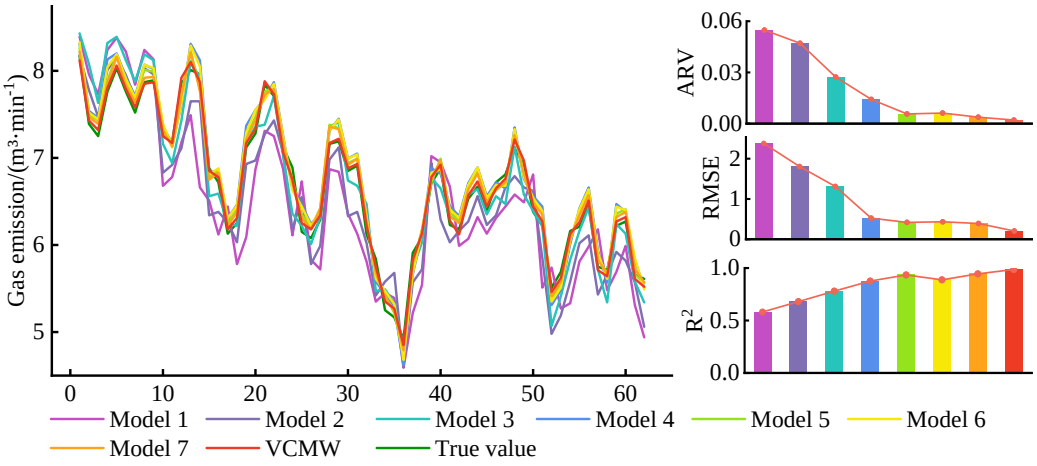

Figure 9. Prediction results of gas emission from different models.

Based on the results of the three-evaluation metrics presented in Table 3 and Figure 9, it can be observed that the prediction performance of the eight models proposed in the comparative experiments gradually improves. By assigning corresponding weights to the errors of LSSVM, WLSSVM shows an improvement in prediction effectiveness compared to LSSVM. Furthermore, when examining Model 3 (SCSO-WLSSVM) and Model 4 (MSCSO-WLSSVM), it becomes evident that the incorporation of the sand cat swarm optimization algorithm enhances the prediction performance of the models. The introduction of the SCSO algorithm, as improved in this paper, further enhances the accuracy of the prediction model. This indicates that optimizing the parameter search of WLSSVM by MSCSO can lead to a certain improvement in the final prediction effectiveness.

Furthermore, upon comparing the prediction results of Model 5 (VMD-MSCSO-WLSSVM) and Model 6 (CEEMDAN-MSCSO-WLSSVM), it can be observed that the introduction

of the VMD signal decomposition technique, yields better prediction results compared to the introduction of CEEMDAN. Both models outperform the first four models in terms of prediction performance. This can be attributed to the signal decomposition technique, which transforms the originally complex sequence into several sub-series with distinct characteristics. VMD technology, in particular, exhibits superior performance in signal decomposition, reducing the complexity of raw data and effectively mitigating issues such as modal aliasing and endpoint effects.

Finally, when comparing the evaluation results of Model 7 (CEEMDAN-VMD-MSCSO-WLSSVM) with Model 8 (VMD-CEEMDAN-MSCSO-WLSSVM), the order of signal decomposition techniques is found to be crucial. Model 7 involves a secondary decomposition of the residual terms obtained from CEEMDAN decomposition using VMD. Although the results show improvement compared to the previous six models, they are not as good as those obtained from Model 8, where the signal is first decomposed using VMD and then CEEMDAN is applied to the secondary decomposition of the VMD residual terms. This indicates that the residual terms obtained after VMD decomposition contain more complex and significant information, and the secondary decomposition process helps simplify the complexity of this information, resulting in improved prediction accuracy for the residual terms and ultimately achieving substantial enhancement in the overall prediction performance of the model.

After analyzing Table 3 and FIGURE 9, it is evident that the prediction model proposed in this paper (VCMW) outperforms other models in predicting methane gas emission using the same dataset. This superiority can be attributed to the effective use of signal decomposition techniques and an improved optimization algorithm. The VCMW model accurately captures the complex patterns of methane gas emission, resulting in higher prediction accuracy. Thus, based on the comprehensive analysis of the results, the VCMW model has the optimal performance for methane gas emission prediction in comparative experiments with the same dataset.

5. **Conclusions.**

In this paper, we proposed a combined prediction model, VMD-CEEMDAN-MSCSO-WLSSVM by introducing secondary decomposition, an improved intelligent optimization algorithm, and the concept of integrated prediction. This model aims to achieve accurate prediction of methane gas emissions. Based on extensive experimental analysis, the following conclusions can be drawn.

- In this study, we employ the decomposition-first and integration-later framework within the complex system methodology. Firstly, gas emission data is decomposed using VMD-CEEMDAN techniques. Next, the optimized prediction model MSCSO-WLSSVM is applied to predict each subseries resulting from the secondary decomposition. Finally, each subseries prediction is combined to obtain the final prediction value. Comparative experimental results demonstrate that our proposed method has significant advantages in terms of prediction performance.
- By incorporating secondary decomposition, the crucial information embedded in the residual terms obtained after VMD decomposition is comprehensively and effectively decomposed using the CEEMDAN method. This enables the extraction of more significant information from the original data, thereby creating favorable conditions for improving the overall performance of the model.
- By incorporating chaotic sequences and the Lévy flight strategy into the SCSO algorithm, the diversity of the population is enhanced and the issue of local optimization is addressed, resulting in improved global search capability and local exploitation

capability. Subsequently, the MSCSO algorithm is applied to optimize the parameters of WLSSVM, leading to the development of the MSCSO-WLSSVM model with improved prediction accuracy and generalization ability.

Due to limitations imposed by objective factors, the dataset chosen for this study exhibits certain constraints. To enhance the generalization capability and accuracy of the model, future endeavors will focus on expanding the sample size. Moreover, the secondary decomposition process generates a multitude of components, potentially impeding training efficiency when addressed individually. Therefore, future efforts will explore component reconstruction techniques aimed at optimizing model training efficiency.

6. **Acknowledgment.** This work is partially supported by the National Natural Science Foundation of China (No.61872126).

REFERENCES

[1] Q. Wu, K. Tu, Y.-F. Zeng and S.-Q. Liu, "Discussion on the main problems and countermeasures for building an upgrade version of the main energy (coal) industry in China," *Journal of China Coal Society*, vol. 44, no. 6, pp. 1625-1636, 2019.

[2] C.-L. Zhang, E.-Y. Wang, Y.-B. Wang and X.-F. Zhou, "Spatial-temporal distribution of outburst accidents from 2001 to 2020 in China and suggestions for prevention and control," *Coal Geology & Exploration*, vol. 49, no. 4, pp. 134–141, 2021.

[3] E.-S. Fu, R.-C. Bai, G.-W. Liu, H. Zhao and C.-D. Yang, "Analysis of characteristics and evolution trend of coal mine accidents in our country during "13th five-year" plan period," *China Safety Science Journal*, vol. 32, no. 12, pp. 88–94, 2022.

[4] W. Wu, "Analysis on the Causes of Coal Mine Accidents and Research on Prevention Countermeasures," in *IOP Conference Series: Earth and Environmental Science*. IOP, 2021, pp. 1–4.

[5] Y.-D. Zhai, "Gas Prediction and Prevention Technology for Mine Mining Areas," *Energy and Energy Conservation*, vol. 2022, no. 7, pp. 127–129, 2022.

[6] G.-L. Wang, "Innovation and management of intelligent mining technology in coal mine," *Shaanxi Coal*, vol. 40, no. S2, pp. 146–149, 2021.

[7] X. Hu, Q. Zheng, X. Huang and K.-H. Yeh, "Revocable and Unbounded Attribute-based Encryption Scheme with Adaptive Security for Integrating Digital Twins in Internet of Things," *IEEE Journal on Selected Areas in Communications*, vol. 14, 3310076, 2023.

[8] X. Hu, H.-X. Wang, W.-Z Meng and K.-H. Yeh, "Attribute-based Data Sharing Scheme with Flexible Search Functionality for Cloud Assisted Autonomous Transportation System," *IEEE Transactions on Industrial Informatics*, 2023. [Online]. Available: https://doi.org/10.1109/TII.2023.3242815

[9] L.-L. Wang, Y. Lin, Y. Ting, X. Hu and K.-T. Liang, "FABRIC: Fast and Secure Unbounded Cross-System Encrypted Data Sharing in Cloud Computing," *IEEE Transactions on Dependable and Secure Computing*, 2023. [Online]. Available: https://doi.org/10.1109/TDSC.2023.3240820

[10] F.-Q. Zhang, T.-Y Wu, Y. Wang, R. Xiong, G.-Y Ding, P. Mei and L.-Y Liu, "Application of quantum genetic optimization of LVQ neural network in smart city traffic network prediction," *IEEE Access*, vol. 8, pp. 104555–104564, 2020.

[11] C.-M. Chen, S. Lv, J.-S Ning and M.-T Wu, "A Genetic Algorithm for the Waitable Time-Varying Multi-Depot Green Vehicle Routing Problem," *Symmetry*, vol. 15, no. 1, 124, 2023.

[12] A.-L. Phulara Shaik, M.-K. Manoharan, A.-K Pani, R.-R Avala and C.-M Chen, "Gaussian Mutation–Spider Monkey Optimization (GM-SMO) Model for Remote Sensing Scene Classification," *Remote Sensing*, vol. 14, no. 24, 6279, 2022.

[13] Y.-S. Xu, J.-N. Bai, Y.-H. Wang, X. Yan and D.-D Wang, "Prediction model of gas emission based on CEEMDAN-DA-GRU," *Chinese Journal of Sensors and Actuators*, vol. 36, no. 3, pp. 441–448, 2023.

[14] F.-L. Wu, Y. Huo and J.-N. Gao, "Coal mine gas emission prediction method based on random forest regression," *Journal of Mine Automation*, vol. 47, no. 8, pp. 102–107, 2021.

[15] L. Dong, S.-Z. Ming, L. Mei, Y.-B Hou, S.-J Mao and Y.-S Niu, "AWLSSVM Gas Prediction Research Based on Chaotic Particle Swarm Optimization," *Applied Bionics and Biomechanics*, vol. 47, no. 8, pp. 193–198, 2020.

[16] J. Chen, J.-W. Ren, X.-W. Zhu, "Result of Direct Determination of Gas Content Prediction Correction Based on WPA- BP Optimized Neural Network," *Coal Technology*, vol. 41, no. 9, pp. 143–147, 2022.

[17] J.-Z. Jia, D.-L. Ke, Y.-N. Chen, "Prediction and forecast of the coal mining gas emission based on the orthogonal test and multiple regression," *Journal of Safety and Environment*, vol. 21, no. 5, pp. 2037–2044, 2021.

[18] P. Jia, S.-L. Sheng, T. Wu and S.-Y Wang, "Forecasting of port container throughput based on TEI@I methodology," *Journal of Systems Science and Mathematical*, vol. 42, no. 12, pp. 3321–3338, 2022.

[19] B. Zeng, J. Guo, F. Zhang, W. Zhu, Z. Xiao, S. Huang and P. Fan, "Borderline-SMOTE: Prediction Model for Dissolved Gas Concentration in Transformer Oil Based on Modified Grey Wolf Optimizer and LSSVM with Grey Relational Analysis and Empirical Mode Decomposition," *Energies*, vol. 13, no. 2, pp. 422–442, 2020.

[20] P.-H. Zhang, D.-W. Li, X.-L. Zhang, "Multi-scale combined prediction of gas concentration based on variational mode decomposition," *Journal of Liaoning Technical University (Natural Science)*, vol. 42, no. 1, pp. 18–24, 2023.

[21] Z.-P. Tang, J.-C. Wu, T.-T. Zhang, X.-X Du and K.-J Chen, "Research on grain futures price forecasting based on secondary decomposition and ensemble learning," *System Engineering Theory and Practice*, vol. 41, no. 11, pp. 2837–2849, 2021.

[22] L. Xiang, J. N. Liu, H. Su, A.-J. Hu and Z.-N. Zhu, "Research on multi-step wind speed forecast based on CEEMDAN secondary decomposition and LSTM," *Acta Energiae Solaris Sinica*, vol. 43, no. 8, pp. 334–339, 2022.

[23] W.-H. Cheng, W.-G. Che, "Research on financial time series forecasting algorithm based on secondary decomposition and LSTM," *Journal of Chongqing University of Posts and Telecommunications (Natural Science Edition)*. vol. 34, no. 4, pp. 638–645, 2022.

[24] H.-F. Lin, "Prediction method and application of gas emission from mining workface based on STL-EEMD GA-SVR," *Coal Geology & Exploration*, vol. 50, no. 12, pp. 131–141, 2022.

[25] K. Dragomiretskiy, D. Zosso, "Variational Mode Decomposition," *IEEE Transactions on Signal Processing*, vol. 62, no. 3, pp. 531–544, 2014.

[26] P.-H. Zhang, D.-W. Li, X.-L. Zhang, "Multi-scale combined prediction of gas concentration based on variational mode decomposition," *Journal of Liaoning Technical University(Natural Science)*, vol. 42, no. 1, pp. 18–24, 2023.

[27] M.-E. Torres, M.-A. Colominas, G. Schlotthauer and P. Flandrin, "A Complete Ensemble Empirical Mode Decomposition With Adaptive Noise," in *International Conference on Acoustics, Speech and Signal Processing - Proceedings (ICASSP)*, IEEE, 2021, pp. 4144-4147.

[28] F. Liu, H.-D. Li, T. Tan, "Short-term wind power prediction based on CEEMDAN-AsyHyperBand-MultiTCN," *Acta Energiae Solaris Sinica*, 2023. [Online]. Available: https://doi.org/10.19912/j.0254-0096.tynxb.2022-1427.

[29] A. Seyyedabbasi, F. Kiani, "Sand Cat swarm optimization: a nature-inspired algorithm to solve global optimization problems," *Engineering with Computers*, vol. 39, no. 4, pp. 2627–2651, 2023.

[30] A. Iraji, J. Karimi, S. Keawsawasvong and M.-L. Nehdi, "Minimum Safety Factor Evaluation of Slopes Using Hybrid Chaotic Sand Cat and Pattern Search Approach," *Sustainability (Basel, Switzerland)*, vol. 14, no. 13, 8097, 2023.

[31] T.-Y. Wu, A.-K. Shao, J.-S. Pan, "CTOA: Toward a Chaotic-Based Tumbleweed Optimization Algorithm," *Mathematics*, vol. 11, no. 10, 2339, 2023.

[32] T.-Y. Wu, H.-N Li, S.-C. Chu, "CPPE: An Improved Phasmatodea Population Evolution Algorithm with Chaotic Maps," *Mathematics*, vol. 11, no. 9, 1977, 2023.

[33] A. Sankalap, A. Priyanka, "Chaotic grasshopper optimization algorithm for global optimization," *Neural Computing and Applications*, vol. 31, no. 8, pp. 4395–4405, 2019.

[34] P. Zhou, C.-Y. Dong, X.-Y. Chen, "An equilibrium optimizer algorithm based on a Tent chaos and lens imaging learning strategy," *Control and Decision*, vol. 38, no. 6, pp. 1569–1576, 2023.

[35] G. Iacca, V.-C. dos Santos Junior and V.-V. de Melo, "An improved Jaya optimization algorithm with Lévy flight," *Expert Systems with Applications*, vol. 165, 113902, 2021.

[36] H.-H Essam, S.-R Mohammed, H.-A Fatma, S. Hassan and M. Hassaballah, "Lévy flight distribution: A new metaheuristic algorithm for solving engineering optimization problems," *Engineering Applications of Artificial Intelligence*, vol. 94, 103731, 2020.

[37] J.-A.-K. Suykens and J. Vandewalle, "Least Squares Support Vector Machine Classifiers," *Neural Processing Letters*, vol. 9, pp. 293–300, 1999.

[38] L. Wang, Y. Liu, Z. Z. Liu and J.-Y. Qi, "Research on prediction model for gas emission based on IABC-LSSVM," *Transducer and Microsystem Technologies*, vol. 41, no. 2, pp. 34–38, 2022.

[39] J.-A.-K Suykens, J. De Brabanter, L. Lukas and J. Vandewalle, "Weighted least squares support vector machines: robustness and sparse approximation," *Neurocomputing (Amsterdam)*, vol. 48, no. 1, pp. 85–105, 2002.

[40] X.-S. Zhang, Y.-Y. Zhang, "Prediction of external corrosion rate of buried pipeline based on KPCA-ALO-WLSSVM," *Journal of Safety and Environment*, vol. 22, no. 4, pp. 1804–1812, 2022.

[41] N. Huang, Y. Wu, G. Cai, H. Zhu, C. Yu, L. Jiang, Y. Zhang, J. Zhang and E. Xing, "Short-Term Wind Speed Forecast with Low Loss of Information Based on Feature Generation of OSVD," *IEEE Access*, vol. 7, no. 1, pp. 81027–81046, 2019.